Int. J. Heat Mass Transfer. Vol. 37, No. 2, pp. 313–319, 1994
Printed in Great Britain

0017–9310/94 $6.00 + 0.00

Simulation of heat transfer to flow in radial grooves of friction pairs

PARVIZ PAYVAR
Northern Illinois University, Department of Mechanical Engineering, DeKalb, IL 60115-2854, U.S.A.

Y. N. LEE
Heat Transfer Research & Development, Ltd., East-West Industrial Co., Inc., 1010 W. Lonnquist Blvd., Mount Prospect, IL 60056, U.S.A.

and

W. J. MINKOWYCZ
The University of Illinois at Chicago, Department of Mechanical Engineering/MC 251, Box 4348, Chicago, IL 60680, U.S.A.

(*Received* 5 *May* 1992 *and in final form* 30 *March* 1993)

Abstract—The naphthalene sublimation technique and numerical solution of the governing equations are used to study the mechanism of heat transfer in the radial grooves of cooled disc friction pairs. It is shown that a main eddy generated by the relative motion of the friction pair creates an effective mechanism of heat transfer to the fluid flowing in the radial grooves. The effect of Coriolis forces and a thin film separating the plates on the heat transfer coefficient are investigated. Numerical and experimental Sherwood numbers for mass transfer agree to within the estimated experimental accuracy of 12%. Sample numerical results are used to describe the detailed behavior of the system.

INTRODUCTION

THE MOTIVATION for the present study is to gain insight into the mechanism of heat transfer to recirculating flow in radial grooves of oil-cooled, disc friction pairs. Payvar [1] has recently studied one application of such friction pairs arising in the design of radially-grooved oil-cooled clutches. The radial grooves are produced by cutting or stamping the paper-based, resin-impregnated friction plate. A major function of the radial grooves is to provide a channel for the flow of oil during continuously slipping operation of the clutch so as to control the temperature of the friction interface. Excessive temperatures will result in oxidation of the transmission oil and failure of the friction material. Figure 1 shows the general flow situation which arises in the grooves. The grooves are idealized as rectangular ducts of constant cross section extending from inner to outer diameter of the friction plate. Fluid enters the duct at the inner diameter with an average velocity w_{in} parallel to the walls of the duct. As the fluid flows radially outward through the duct, the shear forces exerted by the steel separator plate set up a recirculatory motion in the xy-plane superimposed on the motion along the duct. As fluid particles come in contact with the hot separator plate, heat is transferred to them and as they move away from that plate along the three insulated walls, heat is transferred from these particles to the cooler fluid in the core of the recirculation zone.

Figure 2 shows schematically the secondary flow field set up by the relative motion of the discs in the presence of an intervening film of thickness G, in a duct of depth B and width E. The adjoining land is of width L. The fluid flowing in the film is separated from the fluid in the recirculation zone by a dividing streamline. The intensity of recirculation is somewhat reduced due to the presence of the film. Moreover, the

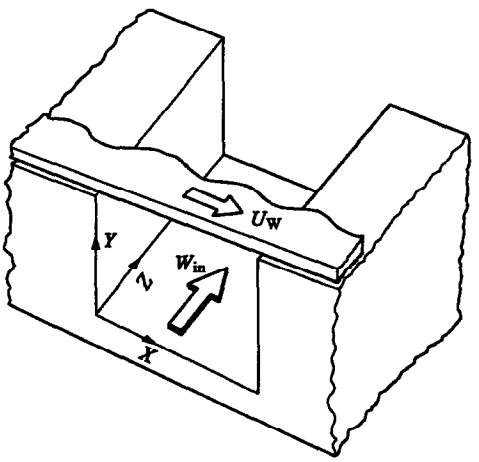

FIG. 1. Schematic diagram of the flow configuration.

NOMENCLATURE

A area used in the definition of mass transfer coefficient
B groove depth
C concentration
D diffusion coefficient
E groove width
G gap thickness
h_m mass transfer coefficient, defined by equation (1)
h_{xz} local mass transfer coefficient, defined by equation (13)
h_z average local mass transfer coefficient, defined by equation (14)
$\bar{h}_z$ overall mass transfer coefficient, defined by equation (15)
L land width
M naphthalene mass evaporated during a test run
N_g number of grooves on the test plate
p pressure
P dimensionless pressure
R_i inner radius of grooved plate
R_o outer radius of grooved plate
Re_f Reynolds number based on flow velocity through the groove, defined by equation (3)
Re_r Reynolds number based on rotational velocity, defined by equation (4)
Sc Schmidt number
Sh_{xz} Sherwood number based on h_{xz}, defined by equation (10)
Sh_z Sherwood number based on h_z, defined by equation (11)
$\overline{Sh}_z$ Sherwood number based on $\bar{h}_z$, defined by equation (12)
t time
u, v, w velocity components
U, V, W dimensionless velocity components
x, y, z Cartesian coordinates
X, Y, Z dimensionless Cartesian coordinates.

Greek symbols
θ dimensionless concentration
ν kinematic viscosity
ρ density
Ω angular velocity.

Subscripts
0 ambient
b bulk
f flow
i inner
in at inlet
LMCD log mean concentration difference
m mass transfer
o outer
r rotational
w at wall
xz local value at x and z
z average local at z.

film acts as a barrier to heat flow from the separator plate to the core fluid since heat must flow through the film essentially by conduction.

Patankar and Spalding [2] have studied the hydrodynamically and thermally developing flow in a duct of square cross section with a laterally moving wall. They presented some flow and heat transfer results for the case of a constant moving wall velocity. Abdel-Wahed *et al.* [3] have reported the fully-developed solution for a duct of square cross section with a constant velocity moving wall. In a clutch application, the moving wall velocity varies linearly with distance along the duct. Furthermore, the intervening film and Coriolis forces, neglected in refs. [2] and [3], play potentially crucial roles in clutch heat transfer.

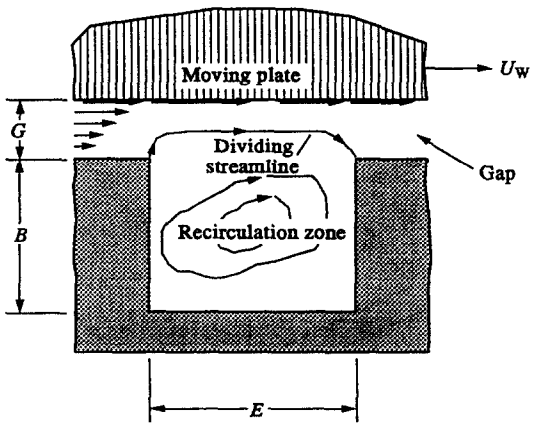

FIG. 2. Relative location and motion of the disc pair.

In the analytical study of the problem, an essential question arises as to whether the flow should be treated as laminar or turbulent. The Reynolds number based on average oil flow velocity and a characteristic length of the groove cross section is normally below 500. In the absence of recirculation imposed by the moving wall, the flow would be laminar. It is assumed in this study that in the presence of recirculation, the flow will be dominated by the main eddy and that any small scale turbulence will have a secondary effect on the magnitude of the heat transfer coefficient. The

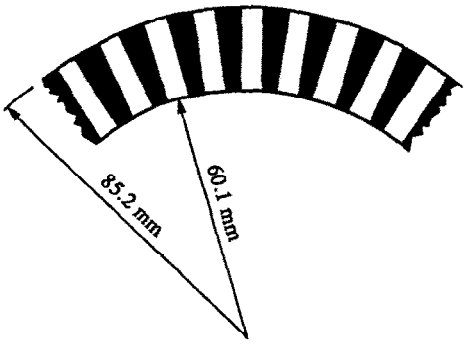

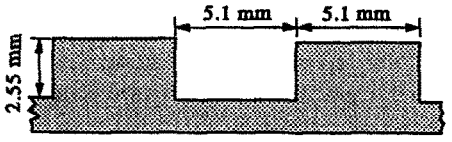

FIG. 3. Top and sectional view of the rectangular grooves.

test for this assumption will be left to experimental verification of the laminar modeling results.

Direct experimental verification of the numerical model through heat transfer experiments is difficult due to the need for temperature measurements at the friction interface. An analogous mass transfer experiment based on the naphthalene technique proved to be a much more practical method to check the validity of the numerical results. In the following sections, the experimental and numerical methods of simulation of the heat transfer problem are described.

EXPERIMENTAL APPARATUS AND PROCEDURE

The desired flow pattern is produced by forcing air through a number of equally spaced rectangular cross section grooves machined in an aluminum disc which is connected to a shaft driven by an electric motor. Just above this rotating disc at a distance of about 0.2 mm is a stationary disc coated with a layer of naphthalene about 0.1 mm thick. Figure 3 shows the top view of the grooved rotating disc as well as the cross section of a single groove and the adjoining land areas. Because it was desired to have grooves of constant cross sectional dimensions, the land width is smaller at the inside diameter of the disc than at the outside diameter. The outside and inside diameters of the discs were 170.4 mm and 120.2 mm, respectively. Each groove was 5.1 mm wide, 2.55 mm deep, and

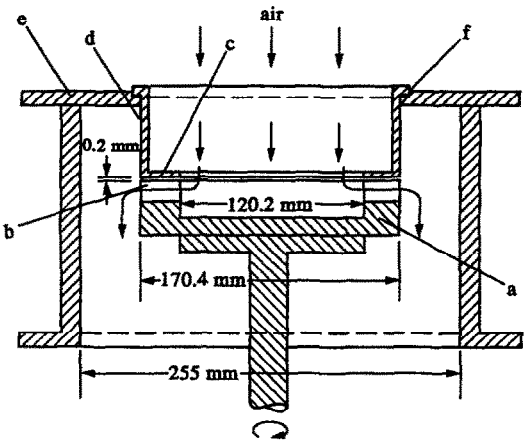

FIG. 4. The naphthalene sublimation test section.

25.1 mm long. There was a total of 45 grooves in the rotating disc.

Figure 4 shows a cross sectional view of the test section. The rotating disc 'a' is shown attached to a shaft driven by a motor. The stationary disc 'c' is attached to a cylinder 'd' which is mounted on a fixed cylinder 'e'. A special spraying technique was used to coat the stationary disc with a layer of naphthalene 0.1 mm thick. The details of this technique are described by Lee [4]. Test air was drawn in by means of an exhauster located downstream of the test section in such a way as to enter the grooves at the inside diameter and exit at the outside diameter. The exhauster discharged the air to outside the laboratory. In order to control the thickness of the film between the two discs, shims 'f' were used. The main features of the test rig are shown in Fig. 5. The test section shown in Fig. 4 is mounted on a platform with the center portion cut out. At the underside of the platform was a leak tight enclosure through which the shaft passed. The shaft was driven by an electric motor via a belt-

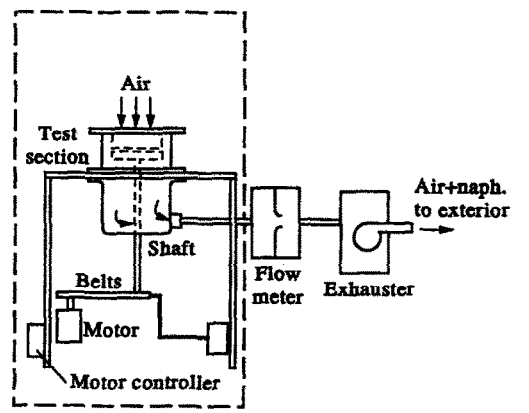

FIG. 5. Schematic diagram of the experimental setup.

pulley system. A special seal was used to prevent leakage between the shaft and the enclosure. The entire system was placed in a laboratory maintained at $25 \pm 1°C$. The dotted line indicates an insulated wooden box inside which the temperature is controlled to within 0.1°C of the set point temperature of 25°C. This was achieved by a separate cooling system in the laboratory. The air passed through the hole in the stationary disc, around the shaft, through the flowmeter and the exhauster to outside the laboratory.

When the temperature of the test section reached its steady state value, the stationary part was weighed with an analytical balance and was immediately installed in the test section. The motor was then started and the system was allowed to run for a period of time Δt. At the end of the time period, the stationary disc was weighed again. The mass of naphthalene sublimed during the time period was determined from the difference between the measurements at the beginning and the end of the time period. Any loss of mass due to the short period of installation or removal of the stationary part was estimated and a correction was applied in order to calculate the net sublimated mass M. Run times were adjusted in each particular test to ensure attainment of the required accuracy. The net sublimated mass M, time period Δt, shaft angular velocity Ω, air flowrate, and the steady state temperature of the enclosure comprised the raw data from which the overall mass transfer coefficient and the two Reynolds numbers were calculated. The mass transfer coefficient h_m is defined as:

$$h_m = \frac{M}{A(\Delta t)(\Delta C)_{LMCD}} \tag{1}$$

where the area A is taken as:

$$A = N_g E(R_o - R_i)$$

and the log mean concentration difference is defined as:

$$(\Delta C)_{LMCD} = \frac{(C_o - C_i)}{\ln\left(\frac{C_o - C_w}{C_i - C_w}\right)}.$$

The overall Sherwood number is defined as:

$$\overline{Sh} = \frac{h_m E}{D}. \tag{2}$$

Two Reynolds numbers are defined. A flow Reynolds number, Re_f, based on the average velocity of flow in the grooves in the z-direction is defined as:

$$Re_f = \frac{w_{in} E}{\nu} \tag{3}$$

and a rotational Reynolds number, Re_r, based on the rotational velocity of the disc at the inside diameter is defined as:

$$Re_r = \frac{R_i \Omega E}{\nu}. \tag{4}$$

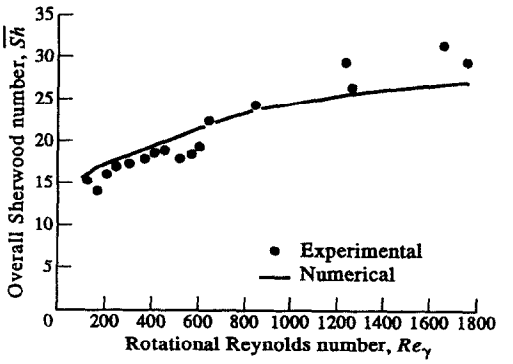

FIG. 6. Comparison of experimental and numerical results. $G/E = 0.04$, $E/R_i = 0.0834$, $Re_f = 480$.

The Schmidt number, ν/D, was calculated as 2.5 for all tests. The gap between the discs was set by use of shims and a special bearing was used to maintain it during the test. Measurements of the gap before and after each test were made to ensure that the gap size did not change during the test. The gap was set at 0.2 mm. Test results are shown in Fig. 6.

MATHEMATICAL FORMULATION

If the diffusion terms in the z-direction are neglected, the governing equations in dimensionless form are,

continuity

$$\frac{\partial U}{\partial X} + \frac{\partial V}{\partial Y} + \frac{\partial W}{\partial Z} = 0 \tag{5}$$

momentum

$$U\frac{\partial U}{\partial X} + V\frac{\partial U}{\partial Y} + W\frac{\partial U}{\partial Z} = -\frac{\partial P}{\partial X} + \frac{1}{Re_r}\nabla^2 U + 2\frac{E}{R_i}\frac{Re_f}{Re_r}W \tag{6}$$

$$U\frac{\partial V}{\partial X} + V\frac{\partial V}{\partial Y} + W\frac{\partial V}{\partial Z} = -\frac{\partial P}{\partial Y} + \frac{1}{Re_r}\nabla^2 V \tag{7}$$

$$U\frac{\partial W}{\partial X} + V\frac{\partial W}{\partial Y} + W\frac{\partial W}{\partial Z} = -\frac{dP^*}{dZ} + \frac{1}{Re_r}\nabla^2 W - 2\frac{E}{R_i}\frac{Re_r}{Re_f}U \tag{8}$$

diffusing species concentration

$$U\frac{\partial \theta}{\partial X} + V\frac{\partial \theta}{\partial Y} + W\frac{\partial \theta}{\partial Z} = \frac{1}{Re_r Sc}\left(\frac{\partial^2 \theta}{\partial X^2} + \frac{\partial^2 \theta}{\partial Y^2}\right) \tag{9}$$

where the following variables and parameters have been used,

$$X = \frac{x}{E}, \quad Y = \frac{y}{E}, \quad Z = \frac{z}{E}\frac{Re_r}{Re_f}$$

$$U = \frac{u}{\Omega R_i}, \quad V = \frac{v}{\Omega R_i}, \quad W = \frac{w}{w_{in}}$$

$$P = \frac{(p - p_0)}{\rho \Omega^2 R_i^2}$$

$$p^* = \frac{p^* - p_0 - \rho(R_i z + \frac{1}{2}z^2)\Omega^2}{\rho w_{in}^2}$$

$$\theta = \frac{C - C_{in}}{C_w - C_{in}}.$$

Note that the longitudinal and lateral pressure gradients have been decoupled by introducing two different dimensionless pressures P and P^*.

The boundary conditions for equations (5)–(9) are,

$$\theta = 0, \quad U = 0, \quad V = 0, \quad W = 1 \quad \text{at} \quad Z = 0.$$

$$\theta = 1, \quad V = 0, \quad W = 0, \quad U = 1 + Z\frac{E}{R_i}\frac{Re_r}{Re_r}$$

$$\text{at} \quad Y = \frac{B+G}{E}.$$

On all other solid boundaries, $U = V = W = 0$, and the gradient of θ normal to the boundary is zero. The domain of calculation extends from the midsection of a land, $X = 0$, to the midsection of the adjoining land, $X = 1 + L/E$. A periodic boundary condition is used at these boundaries. L/E is taken as unity for all the numerical calculations.

In presenting the results, other than the overall Sherwood number defined by equation (2), the following Sherwood numbers are used:

$$Sh_{xz} = \frac{h_{xz}E}{D} \tag{10}$$

$$Sh_z = \frac{h_z E}{D} \tag{11}$$

$$\overline{Sh}_z = \frac{\bar{h}_z E}{D}. \tag{12}$$

h_{xz} in equation (10) is the local mass transfer coefficient defined as:

$$h_{xz} = \frac{-D\left(\frac{\partial C}{\partial y}\right)_{y=0}}{C_w - C_b} \tag{13}$$

while h_z and $\bar{h}_z$ are defined as,

$$h_z = \frac{\int_0^{(L+E)} h_{xz}\,dx}{L+E} \tag{14}$$

$$\bar{h}_z = \frac{M_z E}{D(\Delta C)_{LMCD}} \tag{15}$$

where M_z is the total sublimated mass from $Z = 0$ to Z.

The numerical solution method is presented in the next section followed by results and discussion.

THE NUMERICAL SOLUTION METHOD

The problem formulated in this study is an example of a three dimensional parabolic heat and momentum transfer problem defined by Patankar and Spalding [2]. Their method, with some refinements presented by Patankar [5], was used to discretize the governing equations for U, V, W, and θ. The circular TDMA algorithm, as presented by Patankar *et al.* [6], was used to apply the periodic boundary condition in the x-direction.

Several nonuniform grids and longitudinal step sizes were used to establish independence of the numerical results from the grid and the step size. The difference between the Sherwood numbers calculated by using a 24×20 and a 36×26 cross sectional grid was less than 2%. All final calculations were performed using a 36×26 cross sectional grid and a forward step size of 0.00001 Re_r. The grid nonuniformity was appropriately selected to handle sharp gradients. The residuals in various discretized equations were closely observed during the computations and a sufficient number of iterations were employed to solve all the equations to keep all normalized residuals less than 0.000001. The computer program developed for this study, duplicates the results of Patankar and Spalding [2] and Abdel-Wahed *et al.* [3] to within 1% when their grid size and parameters of calculation are used.

RESULTS AND DISCUSSION

Figure 6 shows a comparison of experimental and numerical results for rotational Reynolds numbers up to 1800. The r.m.s. deviation of the computed overall Sherwood numbers from experimentally measured ones is about 10%. Comparison between numerical and experimental results is somewhat complicated by the rather strong effect of the gap on the overall Sherwood number. To simulate a given experimental run numerically, all the parameters of the experimental run must be measured accurately. The greatest uncertainty in the experiments resulted from the difficulty of measuring the gap dimension G. The overall uncertainty of the experimental Sherwood numbers for a given set of experimental parameters including the gap thickness is estimated to be 12%.

At higher rotational Reynolds numbers, the experimental data fall consistently above the numerically calculated results based on the laminar flow model. The grid size did not have an effect on this behavior. The precise reason for this systematic departure of the two sets of values is unknown. One possible cause may be the effect of partial parabolization in the computations.

Figure 7 shows variation of mean Sherwood number $\overline{Sh}_z$ along the groove. The enhancement of mass transfer due to rotation can be deduced from this figure. Figure 8 shows the variation of overall Sherwood number $\overline{Sh}_z$ when the gap thickness is zero.

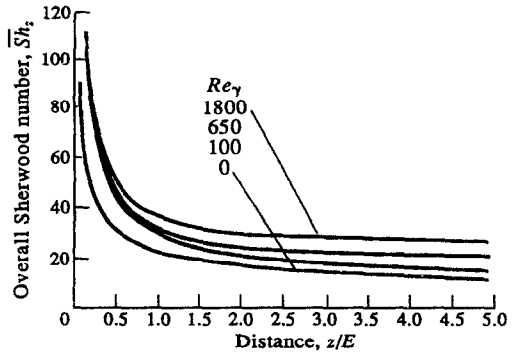

FIG. 7. Variation of overall Sherwood number with distance along the groove. $G/E = 0.04$, $E/R_i = 0.0834$, $Re_r = 480$.

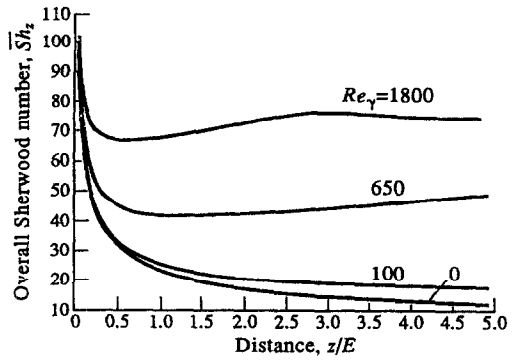

FIG. 8. Variation of overall Sherwood number with distance along the groove. $G/E = 0$, $E/R_i = 0.0834$, $Re_r = 480$.

Comparison with Fig. 7 shows a much greater enhancement of mass transfer with increasing rotational Reynolds number. Figure 9 shows that for thin gaps, i.e. $G/E < 0.01$, mass transfer through the film is essentially by conduction alone and that the

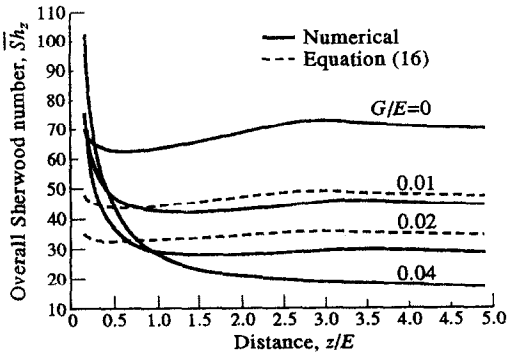

FIG. 9. Variation of overall Sherwood number with distance along the groove. $E/R_i = 0.0834$, $Re_r = 480$, $Re_r = 1800$.

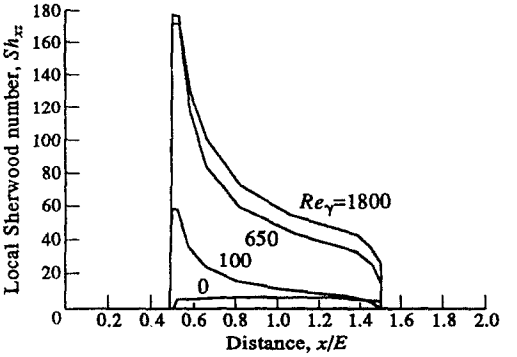

FIG. 10. Variation of local Sherwood number at the exit cross section. $z/E = 5$, $G/E = 0$, $E/R_i = 0.0834$, $Re_r = 480$.

overall Sherwood number can be calculated to within 5% accuracy from the simple formula:

$$Sh_z = \frac{1}{\frac{1}{Sh_{z0}} + \frac{G}{2E}} \tag{16}$$

where Sh_{z0} is the Sherwood number for $G/E = 0$.

Thus for sufficiently small gaps, one only needs to calculate the Sherwood numbers for the much simpler case of $G/E = 0$. In this case, another parameter, the land to groove width ratio L/E, need no longer be considered. This point is also discussed by Payvar [1]. Figure 10 shows the variation of local Sherwood number Sh_{xz} in the groove exit cross section for several values of Re_r. Figures 11 and 12 indicate that for a fixed rotational Reynolds number, as the gap ratio G/E decreases, the contribution of the lands to mass transfer vanishes justifying the use of simple equation (16). The implication of this effect for thermal applications is that the amount of computation needed is enormously reduced due to the possibility of using the simple equation (16). Furthermore, comparison of Figs. 11 and 12 shows that the accuracy of equation (16) is increased as the rotational Reynolds number

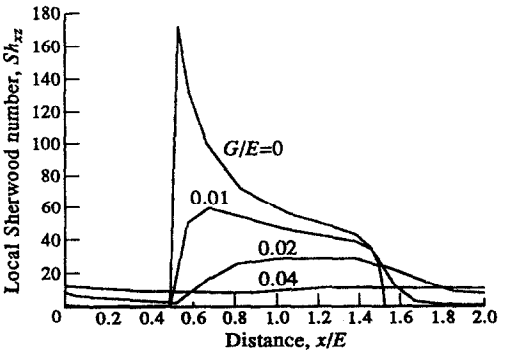

FIG. 11. Variation of local Sherwood number at the exit cross section. $z/E = 5$, $E/R_i = 0.0834$, $Re_r = 480$, $Re_r = 1800$.

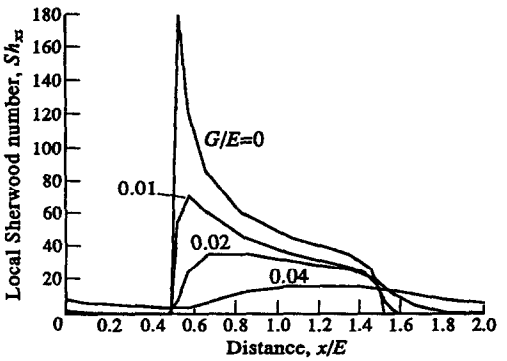

FIG. 12. Variation of local Sherwood number at the exit cross section. $z/E = 5$, $E/R_i = 0.0834$, $Re_f = 480$, $Re_r = 650$.

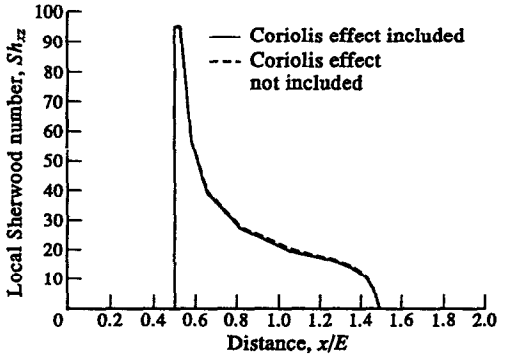

FIG. 13. Effect of Coriolis force on local Sherwood number. $z/E = 5$, $E/R_i = 0.0834$, $Re_f = 480$, $Re_r = 200$.

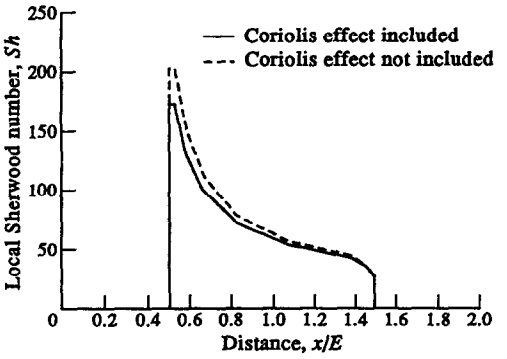

FIG. 14. Effect of Coriolis force on local Sherwood number. $z/E = 5$, $E/R_i = 0.0834$, $Re_f = 480$, $Re_r = 1800$.

and the gap ratio decrease. In practical clutch thermal modeling applications, the gap ratio is always less than 0.01. Figures 13 and 14 show the effect of including or not including the Coriolis forces in the governing equations. The effect of Coriolis forces is to reduce the mass transfer coefficient and the effect is more pronounced at higher rotational Reynolds numbers. For high rotational Reynolds numbers, therefore, clutch designers should consider the benefit of keeping the grooved plate relatively stationary.

CONCLUDING REMARKS

Several important characteristics of the mechanism of heat transfer in radial grooves of disc friction pairs have been presented in this paper. Based on the material presented in the previous section, a practical extension of the research reported in this paper is to calculate Nusselt numbers for a gap ratio of $G/E = 0$ for a range of values of Prandtl number Pr, Reynolds numbers Re_f and Re_r, radius ratio R_o/R_i, and the ratio E/R_i. The simple equation (16) can then be used for calculating the overall Nusselt numbers for small gaps.

Acknowledgement—The authors would like to acknowledge the permission of Borg Warner Corporation to publish the results of this research.

REFERENCES

1. P. Payvar, Laminar heat transfer in the oil groove of a wet clutch, *Int. J. Heat Mass Transfer* **34**, 1791–1798 (1991).
2. S. V. Patankar and D. B. Spalding, Calculation procedure for heat, mass, and momentum transfer in three dimensional parabolic flows, *Int. J. Heat Mass Transfer* **15**, 1787–1806 (1972).
3. R. M. Abdel-Wahed, S. V. Patankar and E. M. Sparrow, Fully-developed laminar flow and heat transfer in a square duct with one moving wall, *Lett. Heat Mass Transfer* **3**, 355–364 (1976).
4. Y. N. Lee, Heat transfer and pressure drop characteristics of an assembly of partially segmented plates, *J. Heat Transfer* **111**, 44–50 (1989).
5. S. V. Patankar, *Numerical Heat Transfer and Fluid Flow*. Hemisphere, New York (1980).
6. S. V. Patankar, C. H. Liu and E. M. Sparrow, Fully-developed flow and heat transfer in ducts having streamwise periodic variation of cross-sectional area, *J. Heat Transfer* **99**, 180–186 (1977).